Competing Orders in the 2D Half-Filled SU(2N) Hubbard Model through the Pinning-Field Quantum Monte Carlo Simulations

Da Wang,[1,*] Yi Li,[1,2] Zi Cai,[3] Zhichao Zhou,[4] Yu Wang,[4,†] and Congjun Wu[1,‡]
[1]Department of Physics, University of California, San Diego, California 92093, USA
[2]Princeton Center for Theoretical Science, Princeton University, Princeton, New Jersey 08544, USA
[3]Department of Physics and Arnold Sommerfeld Center for Theoretical Physics, Ludwig-Maximilians-Universität München, Theresienstraße 37, 80333 Munich, Germany
[4]School of Physics and Technology, Wuhan University, Wuhan 430072, China
(Received 23 May 2013; revised manuscript received 7 February 2014; published 17 April 2014)

We nonperturbatively investigate the ground state magnetic properties of the 2D half-filled SU(2N) Hubbard model in the square lattice by using the projector determinant quantum Monte Carlo simulations combined with the method of local pinning fields. Long-range Néel orders are found for both the SU(4) and SU(6) cases at small and intermediate values of U. In both cases, the long-range Néel moments exhibit nonmonotonic behavior with respect to U, which first grow and then drop as U increases. This result is fundamentally different from the SU(2) case in which the Néel moments increase monotonically and saturate. In the SU(6) case, a transition to the columnar dimer phase is found in the strong interaction regime.

DOI: 10.1103/PhysRevLett.112.156403 PACS numbers: 71.10.Fd, 02.70.Ss, 71.27.+a

The ultracold atom systems have opened up a wonderful opportunity for studying novel phenomena that are not easily accessible in usual solid state systems. For example, the large-spin ultracold alkali-metal and alkaline-earth-metal fermions exhibit quantum magnetic properties fundamentally different from the large-spin solid state systems such as transition metal oxides [1]. In solids, Hund's rule coupling combines several electrons on the same cation site into states carrying large spin S. However, the symmetry of these systems is usually only SU(2). The leading order coupling between two neighboring sites is mediated by exchanging one pair of electrons no matter how large S is; thus, quantum spin fluctuations are suppressed by the $1/S$ effect. In contrast, large-hyperfine-spin ultracold fermion systems which means thats of SU(2N) and Sp(2N). For the simplest case of spin $\frac{3}{2}$, a generic Sp(4) symmetry was proved without fine tuning, which includes the SU(4) symmetry as a special case [2]. Such a high symmetry gives rise to exotic properties in quantum magnetism and pairing superfluidity [3–12]. Furthermore, large-spin alkaline-earth-metal fermion systems have been experimentally realized in recent years [13–15]. In particular, a SU(6) Mott insulator of ^{173}Yb has also been observed [1,16]. The above theoretical and experimental progress has stimulated a great deal of interest in exploring novel properties of strongly correlated systems with high symmetries [17–23].

The SU(2N) Heisenberg model was first introduced into condensed matter physics to apply the large-N technique to systematically handle strong correlation effects in the context of high T_c cuprates [24–28]. It was found that on 2D bipartite lattices the SU(2) Heisenberg model displays long-range Néel ordering [29]. As $2N$ increases, enhanced quantum fluctuations suppress Néel ordering and the ground states eventually become dimerized [27,28]. This transition has been observed by quantum Monte Carlo (QMC) simulations [30–35] for certain representations of the SU(2N) symmetry [36]. However, for the self-conjugate representations, a consensus has not been achieved yet. A variational Monte Carlo study [34] found Néel ordering when $2N = 2$ and 4, and columnar dimer ordering for $2N \geq 6$. However, in a determinant QMC calculation [35], dimer ordering was found at $2N \geq 6$ in agreement with the variational QMC study, while for the SU(4) case, neither Néel nor dimer ordering exists in the Heisenberg limit.

The above Heisenberg-type models neglect charge fluctuations. The interplay between charge and spin degrees of freedom is contained in the SU(2N) Hubbard model [21,37,38]. However, owing to the lack of nonperturbative methods, the SU(2N) Hubbard model receives much less attention. To the best of our knowledge, a systematic nonperturbative study of the ground state properties of the 2D half-filled models is still missing. It is even not clear whether Néel or dimer ordering exists in the weak-, intermediate-, and strong-coupling regimes, respectively.

In this Letter, we perform a nonperturbative determinant QMC study on the half-filled SU(2N) Hubbard model in the 2D square lattice. The ground state magnetic properties are investigated by using the local pinning-field method, which directly measures the spatial decay of the induced order parameters [39]. Long-range Néel order is identified at weak and intermediate values of U in the SU(2N) Hubbard models of $2 \leq 2N \leq 6$ we studied. In the cases of SU(4) and SU(6), the Néel moments first grow then drop with increasing U. Furthermore, a transition from the Néel-ordering phase into the columnar dimer-ordering phase is observed at a large value of U in the SU(6) case. This transition is conceivably owing to the competition between

the weak-coupling physics of Fermi surface nesting and strong coupling local moment physics.

We consider the SU($2N$) Hubbard model in the 2D square lattice with the periodic boundary condition as

$$H = -t\sum_{\langle i,j\rangle,\alpha}(c^{\dagger}_{i\alpha}c_{j\alpha} + \text{H.c.}) + \frac{U}{2}\sum_{i}(n_i - N)^2, \quad (1)$$

where t is the nearest neighbor hopping integral ($t = 1$ below); U is the on-site repulsion; α is the spin index running from 1 to $2N$; $n_i = \sum_{\alpha=1}^{2N} n_{i\alpha}$ is the total fermion number operator on site i. Equation (1) possesses the particle-hole symmetry $c_{i\alpha} \to (-1)^i c^{\dagger}_{i\alpha}$, which means that it is at half filling. In this case, it is well-known that Eq. (1) is free of the sign problem for all the values of N.

We employ the projector QMC method to investigate its quantum magnetic properties in the ground states. In QMC studies, the long-range ordering is usually obtained through the finite-size scaling of the corresponding structural factors, or, correlation functions. Assuming that the system size is $L \times L$, the extrapolated values as $L \to \infty$ are proportional to the magnitude square of order parameters. Thus it is difficult to distinguish the weakly ordered states from the truly disordered ones. For this reason, there has been a debate whether a quantum spin liquid phase exists near the Mott transition in the honeycomb lattice [40–44]. To overcome this difficulty, we use the pinning-field method [39,44], and measure the spatial decay of the induced order parameters. Order parameters instead of their magnitude square are measured, and thus numerically they are more sensitive to weak orderings. This method has also been used in the projector QMC method recently [44]. To decouple the interaction term, we adopt the Hubbard-Stratonovich transformation in the density channel, which involves complex numbers [45]. We have designed a new discrete Hubbard-Stratonovich decomposition that is exact for the cases from SU(2) to SU(6) Hubbard models, and the algorithm details can be found in the Supplemental Material [46]. Unless specifically stated, the following parameters are used in simulations: the projection time $\beta = 240$ and the discretized imaginary time step $\Delta\tau = 0.05$.

Next we use the pinning-field method to study the magnetic long-range order of the SU($2N$) Hubbard model. We define the SU($2N$) generators as $S_i^{\alpha\beta} = c^{\dagger}_{i,\alpha}c_{i,\beta} - (\delta^{\alpha\beta}/2N)n_i$. At half filling, in the Heisenberg limit in which charge fluctuations are neglected, each site belongs to the self-conjugate representation with one column of N boxes. Without loss of generality, the classic Néel state configuration can be chosen as follows: each site in sublattice A is filled with N fermions from components 1 to N, while that in sublattice B is filled with components from $N+1$ to $2N$. We define the magnetic moment operator on each site i as

$$m_i = \frac{1}{2N}\left\{\sum_{\alpha=1}^{N} S_i^{\alpha\alpha} - \sum_{\alpha=N+1}^{2N} S_i^{\alpha\alpha}\right\}. \quad (2)$$

For the configuration defined above, the value of the classic Néel moment is $m_i = (-1)^i\frac{1}{2}$. Within the zero temperature projector QMC method, good quantum numbers are conserved during the projection. Thus we use a pair of pinning fields on two neighboring sites with a Néel configuration to maintain the relation $\langle G|\sum_i S_i^{\alpha\alpha}|G\rangle = 0$ for every α. The pinning-field Hamiltonian is

$$H_{\text{pin},n} = 2Nh_{i_0j_0}\{m_{i_0} - m_{j_0}\}, \quad (3)$$

where i_0 and j_0 are two neighboring sites defined as $i_0 = (1,1)$ and $j_0 = (2,1)$, respectively. The initial trial wave functions can be chosen as the half-filled plane-wave states. The Hamiltonian Eq. (1) plus Eq. (3) remains free of the sign problem at half filling.

Because the pinning fields in Eq. (2) break the SU($2N$) symmetry, the induced magnetic moments prefer the direction defined in Eq. (2). The distribution of m_i is staggered with decaying magnitudes as away from two pinned sites i_0 and j_0. The Néel order parameter is its Fourier component at the wave vector $Q = (\pi,\pi)$ defined as $m_Q(L) = (1/L^2)\sum_i(-1)^i m_i$. The long-range order m_Q can be extrapolated as the limit of

$$m_Q = \lim_{L\to\infty} m_Q(L). \quad (4)$$

This is because the Fourier component of the pinning field at Q is $h_Q = 2h_{i_0j_0}/L^2$, which goes to zero as $L \to \infty$ for any finite value of $h_{i_0j_0}$.

To illustrate the sensitivity of the pinning-field method to weak orders, we present the simulations for the SU(6) case of Eq. (1) with $U = 4$. The finite-size scalings of $m_Q(L)$ are presented in Fig. 1 for two different values of $h_{i_0j_0} = 1$ and 2. Their extrapolated values as $1/L \to 0$ are 0.0261 ± 0.0008 and 0.0253 ± 0.0009, respectively, which are consistent with each other and confirm the validity of this method. Such a small moment is hard to identify using the finite size scaling of the structural factors, as shown in the Supplemental Material [46] and related works [40,42,44]. Another observation is that the induced values of $m_Q(L)$

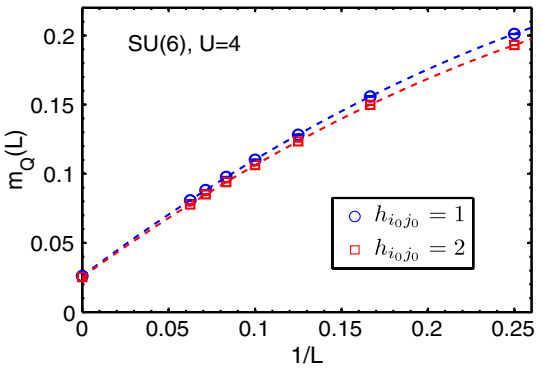

FIG. 1 (color online). Finite size scaling of the residual Néel moment $m_Q(L)$ vs $1/L$ under pinning fields described by Eq. (3) with $h_{i_0j_0} = 1$ and 2. The largest value of L is 16. The quadratic polynomial fitting is used. Error bars are smaller than symbols.

are weaker at $h_{i_0j_0} = 2$ than those at $h_{i_0j_0} = 1$ at finite values of L, which shows nonlinear correlations between the pinning centers and the measured sites. Certainly they converge in the limit of $1/L \to 0$. In the following, we only present the results of $h_{i_0j_0} = 2$.

One may question whether the pinning-field method overestimates the tendency of long-range ordering. In the Supplemental Material [46], we apply it to the 1D SU(2) and SU(4) Hubbard chains at half filling. In the SU(2) case, the ground state is known as a gapless spin liquid, while in the SU(4) case, it is gapped with dimerization. The pinning-field method shows the absence of long-range Néel ordering in both cases and the asymptotic behavior of power-law spin correlations in the case of SU(2). This further confirms the validity of this method.

We further test the validity of the pinning-field method in the extensively studied half-filled SU(2) Hubbard model in the square lattice by the QMC method [47,48]. The long-range Néel ordering we obtained based on the pinning-field method is consistent with that in previous QMC literature based on the finite-size scaling of structure factors. Our results are shown in the Supplemental Material [46]. The long-range Néel ordering appears from weak to strong interactions. The extrapolated values of m_Q increase as U goes up, and begin to saturate around $U = 10$. At $U = 20$, $m_Q = 0.297 \pm 0.002$, which is in a good agreement with the long-range Néel moment 0.3070(3) of the SU(2) Heisenberg model [49]. This behavior is well known [47,48]: as U goes up, charge fluctuations are suppressed, and thus the low energy physics is described by the Heisenberg model.

Next we simulate the SU(4) Hubbard model, and the magnetic ordering is presented in Fig. 2. Similarly to the SU(2) case, long-range Néel ordering appears for all the values of $U \leq 20$. At each value of U, the extrapolated long-range Néel moment m_Q is weaker than that in the SU(2) case, which is a result of the enhanced quantum fluctuations. Moreover, a striking new feature appears: the relation m_Q vs U becomes nonmonotonic as shown in Fig. 4 below. The Néel moment m_Q reaches the maximum around 0.178 ± 0.008 at $U \approx 8$, and then decreases as U further increases. It remains finite with the largest value of $U = 20$ in our simulations. It is not clear whether m_Q is suppressed to zero or not in the limit of $U \to \infty$. A previous QMC simulation on the SU(4) Heisenberg model shows algebraic spin correlations [35]. It would be interesting to further investigate whether the algebraic spin liquid state survives at finite values of U.

With further increases in $2N$, the Néel ordering is more strongly suppressed by quantum spin fluctuations. The finite-size scalings for the SU(6) case at different values of U are presented in Fig. 3. For all the values of $U \leq 14$, we find nonzero Néel ordering by using the quadratic polynomial fitting. The extrapolated Néel moments m_Q vs U for the SU(6) case are plotted in Fig. 4. For comparison, those of the SU(2) and SU(4) are also plotted together. Similar to the SU(4) case, the long-range Néel moments are

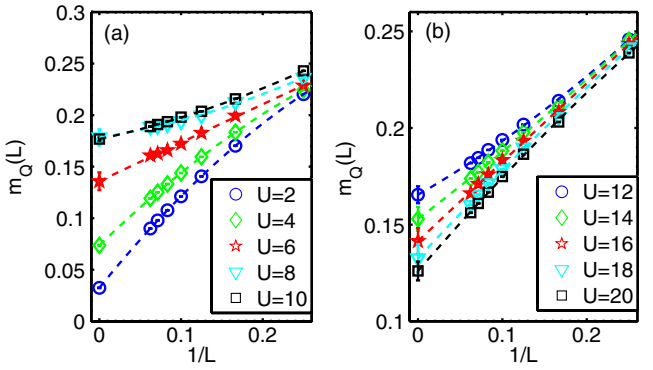

FIG. 2 (color online). Finite size scalings of $m_Q(L)$ vs $1/L$ for the half-filled SU(4) Hubbard model with different values of U. The largest size is $L = 16$. The quadratic polynomial fitting is used. Error bars of QMC data are smaller than symbols.

nonmonotonic, which reach the maximum around $U \approx 10$. Strikingly, the Néel ordering disappears beyond a critical value of U_c, which is estimated as $14 < U_c < 16$.

The low energy effective model of half-filled Hubbard models in the strong-coupling regime is the Heisenberg model. According to the large-N study of the SU($2N$) Heisenberg model with the self-conjugate 1^N representation [27,28], dimerization appears in the large-N limit. Thus the suppression of the Néel order at large values of U is expected from the competing dimer ordering. To investigate this competition, we further apply the pinning-field method to study the dimer ordering for the SU(6) Hubbard model, and the results are presented in Fig. 5. The following dimer pinning field is applied, which changes the hopping integral of a bond i_0j_0 [50],

$$H_{\text{pin,dim}} = -\Delta t_{i_0j_0} \sum_{\alpha} \{c^{\dagger}_{i_0,\alpha} c_{j_0,\alpha} + \text{H.c.}\}, \qquad (5)$$

where i_0 and j_0 are defined as before. The bonding strength between sites i and $i+\hat{x}$ is defined as $d_{i,x} = \frac{1}{2}\langle G|c^{\dagger}_{i\alpha} c_{i+x,\alpha} + \text{H.c.}|G\rangle$, where $|G\rangle$ is the ground

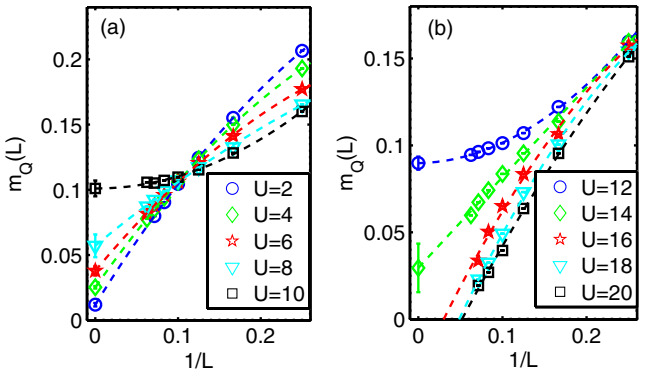

FIG. 3 (color online). Finite size scalings of $m_Q(L)$ vs $1/L$ for the SU(6) Hubbard model at different values of U. The largest size is $L = 16$. The quadratic polynomial fitting is used. Error bars of QMC data are smaller than symbols.

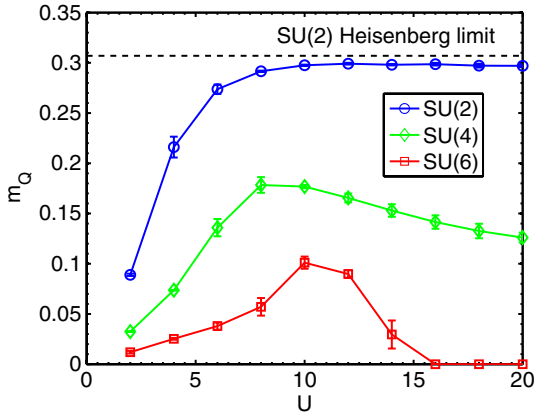

FIG. 4 (color online). The ground state Néel ordering of the 2D half-filled SU($2N$) Hubbard model in the square lattice. The relations of long-range Néel moments m_Q vs U are plotted for $2N = 2$, 4, and 6. For comparison, the SU(2) Heisenberg limit result is plotted as the dotted line. The error bars are obtained from the least square fittings with 95% confidence bounds.

state. We define the dimer order parameter at the wave vector $(\pi, 0)$ as

$$\mathrm{dim}_{(\pi,0)}(L) = \frac{1}{L^2}\sum_i (-1)^{i_x} d_{i,x}, \tag{6}$$

where i_x is the x coordinate of site i. Following the same reasoning to extrapolate the long-range Néel ordering as before, we define the long-range dimer order parameter as $\mathrm{dim}_{(\pi,0)} = \lim_{L\to\infty} \mathrm{dim}_Q(L)$. The finite-size scalings for $\mathrm{dim}_{(\pi,0)}(L)$ are plotted in Fig. 5(a), which shows that the columnar dimerization appears when U is above a critical value U_c', which is also estimated around 14–16. It lies in the same interaction regime that Néel ordering starts to vanish. However, whether this transition is of second order such that $U_c = U_c'$ or it is of first order still needs further numeric investigation. We also measure the dimerization at $Q = (\pi, \pi)$ induced by the pinning-field Eq. (5), defined as $\mathrm{dim}_{(\pi,\pi)}(L) = (1/L^2)\sum_i (-1)^i d_{i,x}$, whose finite-size scaling shows the absence of long-range order.

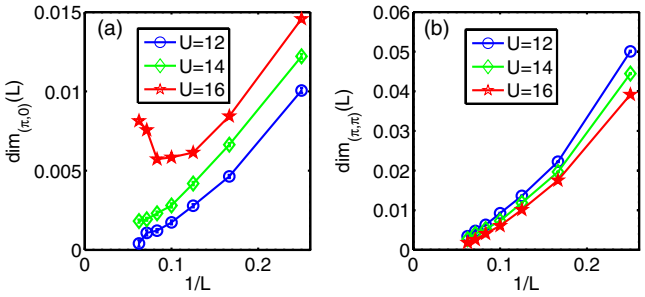

FIG. 5 (color online). Finite-size scalings of the dimer order parameters in the half-filled SU(6) Hubbard model. (a) $\mathrm{dim}_{(\pi,0)}(L)$ and (b) $\mathrm{dim}_{(\pi,\pi)}(L)$ at wave vectors $Q' = (\pi, 0)$ and $Q = (\pi, \pi)$, respectively. The largest size is $L = 16$. Error bars of QMC data are smaller than symbols.

The nature of the transition between the Néel and dimer orderings is an interesting question. In the literature [51,52], ring exchange terms are added to the SU(2) Heisenberg model, which suppress Néel ordering and lead to dimerization. However, our SU(6) case is dramatically different. The SU(6) Néel ordering appears in the regime of weak and intermediate interactions. In this regime ring exchanges are prominent because they reflect short-range charge fluctuations. Our results agree with the picture of Fermi surface nesting because the Néel ordering wave vector $Q = (\pi, \pi)$ is commensurate with the Fermi surface at half filling, while dimerization is not favored because its wave vector $Q' = (\pi, 0)$ does not satisfy the nesting condition [53]. On the other hand, local moment physics dominates when deeply inside the Mott insulating phase in the strong-coupling regime. The exchange energy per site in the dimerized phase is estimated at the order of N^2J with $J = 4t^2/U$, while that of the Néel state is zNJ, where z is the coordination number. Thus dimerization wins when both conditions of large-U and large-N limits are met in agreement with previous theoretical results on SU($2N$) Heisenberg models [27].

Summary.—We have applied the method of local pinning fields in QMC simulations to investigate quantum magnetic properties of the 2D half-filled SU($2N$) Hubbard model in the square lattice. This method is sensitive to weak long-range orders. Long-range Néel ordering is found for the SU(4) case from weak to strong interactions. For the SU(6) case, a transition from the staggered Néel ordering to the columnar dimerization is found as increasing U. The conceivable mechanism is the competition between the weak-coupling Fermi surface nesting physics and the strong-coupling local moment physics. The above QMC simulations may provide a reference point for further investigating the even more challenging problem of doped SU($2N$) Mott insulators.

We thank J. E. Hirsch and Y. Wan for helpful discussions. Especially, we thank H. H. Hung for providing numeric results from exact diagonalizations for comparison. D. W., Y. L., and C. W. are supported by NSF DMR-1105945 and AFOSR FA9550-11-1-0067(YIP); Z. C. thanks the German Research Foundation through DFG FOR 801. Z. Z., Y. W., and C. W. acknowledge financial support from the National Natural Science Foundation of China (11328403, J1210061), and the Fundamental Research Funds for the Central Universities. Y. L. thanks support from the Inamori Fellowship and additional support from the Princeton Center for Theoretical Science. We acknowledge support from the Center for Scientific Computing from the CNSI, MRL: an NSF MRSEC (DMR-1121053) and NSF CNS-0960316.

*d6wang@physics.ucsd.edu
†yu.wang@whu.edu.cn
‡wucj@physics.ucsd.edu

[1] C. Wu, Nat. Phys. **8**, 784 (2012).

[2] C. Wu, J.-P. Hu, and S.-C. Zhang, Phys. Rev. Lett. **91**, 186402 (2003); C. Wu, Mod. Phys. Lett. B **20**, 1707 (2006).
[3] C. Wu, Phys. Rev. Lett. **95**, 266404 (2005).
[4] K. Hattori, J. Phys. Soc. Jpn. **74**, 3135 (2005).
[5] P. Lecheminant, E. Boulat, and P. Azaria, Phys. Rev. Lett. **95**, 240402 (2005).
[6] D. Controzzi and A. M. Tsvelik, Phys. Rev. Lett. **96**, 097205 (2006).
[7] M. A. Cazalilla, A. F. Ho, and M. Ueda, New J. Phys. **11**, 103033 (2009).
[8] C. Wu, J.-P. Hu, and S.-C. Zhang, Int. J. Mod. Phys. B **24**, 311 (2010).
[9] K. Rodríguez, A. Argüelles, M. Colomé-Tatché, T. Vekua, and L. Santos, Phys. Rev. Lett. **105**, 050402 (2010).
[10] P. Corboz, A. M. Läuchli, K. Penc, M. Troyer, and F. Mila, Phys. Rev. Lett. **107**, 215301 (2011).
[11] H.-H. Hung, Y. Wang, and C. Wu, Phys. Rev. B **84**, 054406 (2011).
[12] E. Szirmai and M. Lewenstein, Europhys. Lett. **93**, 66005 (2011).
[13] B. J. DeSalvo, M. Yan, P. G. Mickelson, Y. N. Martinez de Escobar, and T. C. Killian, Phys. Rev. Lett. **105**, 030402 (2010).
[14] S. Taie, Y. Takasu, S. Sugawa, R. Yamazaki, T. Tsujimoto, R. Murakami, and Y. Takahashi, Phys. Rev. Lett. **105**, 190401 (2010).
[15] J. S. Krauser, J. Heinze, N. Fläschner, S. Götze, O. Jürgensen, D.-S. Lühmann, C. Becker, and K. Sengstock, Nat. Phys. **8**, 813 (2012).
[16] S. Taie, R. Yamazaki, S. Sugawa, and Y. Takahashi, Nat. Phys. **8**, 825 (2012).
[17] M. Hermele, V. Gurarie, and A. M. Rey, Phys. Rev. Lett. **103**, 135301 (2009).
[18] A. V. Gorshkov, M. Hermele, V. Gurarie, C. Xu, P. S. Julienne, J. Ye, P. Zoller, E. Demler, M. D. Lukin, and A. M. Rey, Nat. Phys. **6**, 289 (2010).
[19] Z. Cai, H.-H. Hung, L. Wang, D. Zheng, and C. Wu, Phys. Rev. Lett. **110**, 220401 (2013).
[20] L. Messio and F. Mila, Phys. Rev. Lett. **109**, 205306 (2012).
[21] Z. Cai, H.-H. Hung, L. Wang, and C. Wu, Phys. Rev. B **88**, 125108 (2013).
[22] G. Szirmai, E. Szirmai, A. Zamora, and M. Lewenstein, Phys. Rev. A **84**, 011611 (2011).
[23] P. Sinkovicz, A. Zamora, E. Szirmai, M. Lewenstein, and G. Szirmai, Phys. Rev. A **88**, 043619 (2013).
[24] I. Affleck, Phys. Rev. Lett. **54**, 966 (1985).
[25] D. P. Arovas and A. Auerbach, Phys. Rev. B **38**, 316 (1988).
[26] I. Affleck and J. B. Marston, Phys. Rev. B **37**, 3774 (1988).
[27] N. Read and S. Sachdev, Nucl. Phys. **B316**, 609 (1989).
[28] N. Read and S. Sachdev, Phys. Rev. Lett. **62**, 1694 (1989).
[29] P. W. Anderson, Phys. Rev. **86**, 694 (1952).
[30] K. Harada, N. Kawashima, and M. Troyer, Phys. Rev. Lett. **90**, 117203 (2003).
[31] N. Kawashima and Y. Tanabe, Phys. Rev. Lett. **98**, 057202 (2007).
[32] K. S. D. Beach, F. Alet, M. Mambrini, and S. Capponi, Phys. Rev. B **80**, 184401 (2009).
[33] R. K. Kaul and A. W. Sandvik, Phys. Rev. Lett. **108**, 137201 (2012).
[34] A. Paramekanti and J. B. Marston, J. Phys. Condens. Matter **19**, 125215 (2007).
[35] F. F. Assaad, Phys. Rev. B **71**, 075103 (2005).
[36] The representations of $SU(2N)$ are classified by the Young tableau. On a bipartite lattice, the two sublattices can realize two different representations of the $SU(2N)$ group that are complex conjugates to each other, such that two neighboring sites can form a $SU(2N)$ invariant singlet. The system can be simply thought of as loading m fermions per site in the A sublattice and $2N - m$ fermions per site in the B sublattice. The case of $m = 1$ was investigated in Refs. [30–33]. While the case of $m = N$, which forms the self-conjugate representation, was studied in Refs. [34,35].
[37] J. P. Lu, Phys. Rev. B **49**, 5687 (1994).
[38] C. Honerkamp and W. Hofstetter, Phys. Rev. Lett. **92**, 170403 (2004).
[39] S. R. White and A. L. Chernyshev, Phys. Rev. Lett. **99**, 127004 (2007).
[40] Z. Y. Meng, T. C. Lang, S. Wessel, F. F. Assaad, and A. Muramatsu, Nature (London) **464**, 847 (2010).
[41] T. Li, Europhys. Lett. **93**, 37007 (2011).
[42] S. Sorella, Y. Otsuka, and S. Yunoki, Sci. Rep. **2**, 992 (2012).
[43] S. R. Hassan and D. Sénéchal, Phys. Rev. Lett. **110**, 096402 (2013).
[44] F. F. Assaad and I. F. Herbut, Phys. Rev. X **3**, 031010 (2013); F. F. Assaad, private communication (2012).
[45] J. E. Hirsch, Phys. Rev. B **28**, 4059 (1983).
[46] See Supplemental Material at http://link.aps.org/supplemental/10.1103/PhysRevLett.112.156403, which includes Refs. [54–56].
[47] J. E. Hirsch, Phys. Rev. B **31**, 4403 (1985).
[48] C. Varney, C.-R. Lee, Z. Bai, S. Chiesa, M. Jarrell, and R. Scalettar, Phys. Rev. B **80**, 075116 (2009).
[49] A. W. Sandvik, Phys. Rev. B **56**, 11678 (1997).
[50] The kinetic energy dimerization, i.e., the staggered ordering of bonding strength, is equivalent to spin dimerization in the large-U limit. In the background of half-filled Mott insulating states, the kinetic energy on each bond vanishes at the first order perturbation theory. Its effect begins to appear at the second order as the antiferromagnetic spin-spin coupling.
[51] T. Senthil, A. Vishwanath, L. Balents, S. Sachdev, and M. P. A. Fisher, Science **303**, 1490 (2004).
[52] A. W. Sandvik, Phys. Rev. Lett. **98**, 227202 (2007).
[53] Even though the $Q = (\pi, \pi)$ nesting vector allows for commensurate dimerization, there appears a vertex function $f_d(k) = \sin k_x$ in the expression of its susceptibility $\chi_{\mathrm{dim}}(Q) = -\mathrm{Tr}(G(k) f_d(k) G(k+Q) f_d(k+Q))$, where $G(k)$ is the free Green's function. The susceptibility for the Néel ordering shares the same expression by substituting the vertex function with $f_N(k) = 1$. The low energy density of states concentrate around points of van Hove singularity located at $(\pm\pi, 0)$ and $(0, \pm\pi)$ at which the vertex function $f_d(k)$ vanishes. Thus the angular dependences of vertex functions suppress the dimer ordering but favor Néel ordering at $Q = (\pi, \pi)$ in the weak-coupling regime.
[54] F. F. Assaad and H. G. Evertz, *Computational Many-Particle Physics* Lecture Notes in Physics Vol. 739 (Springer, New York, 2008).
[55] C. Wu and S.-C. Zhang, Phys. Rev. B **71**, 155115 (2005).
[56] H. J. Schulz, Phys. Rev. Lett. **64**, 2831 (1990).

Supplementary Material on "Competing orders in the 2D half-filled SU(2N) Hubbard model through the pinning field quantum Monte-Carlo simulations"

Da Wang, Yi Li, Zi Cai, Zhichao Zhou, Yu Wang, and Congjun Wu

In this supplementary material, we explain the algorithm of the projector quantum Monte Carlo method in Sect. I. Various tests of the local pinning field method are presented in Sect. II. The error analysis is performed in Sect. III.

I. PROJECTOR QUANTUM MONTE CARLO AND HUBBARD-STRATONOVICH DECOMPOSITION

We adopt the projector determinant QMC method[1] to study the half-filled SU($2N$) Hubbard model. The basic idea is to apply the projection operator $\mathrm{e}^{-\beta H/2}$ on a trial wave function $|\Psi_T\rangle$. If $\langle\Psi_G|\Psi_T\rangle \neq 0$ and there exists a nonzero gap between $|\Psi_G\rangle$ and the first excited state, $|\Psi_G\rangle$ is arrived as the projection time $\beta \to \infty$,

$$|\Psi_G\rangle = \lim_{\beta\to\infty} \mathrm{e}^{-\beta H/2}|\Psi_T\rangle. \quad (1)$$

The projection time β can be divided into M slices with $\beta = M\Delta\tau$.

The second order Suzuki-Trotter decomposition is used to separate the kinetic and interaction energy parts in each time slice,

$$\mathrm{e}^{-\Delta\tau(K+V)} = \mathrm{e}^{-\Delta\tau K/2}\mathrm{e}^{-\Delta\tau V}\mathrm{e}^{-\Delta\tau K/2} + o[(\Delta\tau)^3], \quad (2)$$

where K and V represent the kinetic and interaction terms, respectively. For the V term, a discrete Hubbard-Stratonovich (HS) transformation is defined as[2]

$$e^{-\lambda^2(n_i-N)^2} = \frac{1}{4}\sum_{l=\pm1,\pm2}\gamma_i(l)e^{i\eta_i(l)(n_i-N)} + o[(\Delta\tau)^4], \quad (3)$$

where $n_i = \sum_{\alpha=1}^{2N} c_{i\alpha}^\dagger c_{i\alpha}$; $\lambda = \sqrt{\Delta\tau U/2}$; γ's and η's are discrete HS fields given by the following values[3]

$$\begin{aligned}
&\gamma(\pm1) = 1 + \frac{\sqrt{6}}{3}, \qquad \gamma(\pm2) = 1 - \frac{\sqrt{6}}{3},\\
&\eta(\pm1) = \pm\sqrt{\Delta\tau U}\sqrt{3-\sqrt{6}},\\
&\eta(\pm2) = \pm\sqrt{\Delta\tau U}\sqrt{3+\sqrt{6}}.
\end{aligned} \quad (4)$$

This decomposition is widely used in QMC simulations[3,4]. However, one should be careful that at large values of U and $|n-N|$ in Eq. 3. In Fig. 1, we plot the values of the left and right hand sides of Eq. 3 as functions of $\Delta\tau U$ for comparison. We consider the situations of $|n-N| = 1, 2$ and 3, respectively. The errors of this discrete HS decomposition Eq. 4 depend on $|n-N|$ significantly. At $|n-N| = 1$ and 2, the decomposition yields values almost exact, or, with slight deviations for $\Delta\tau U < 1$. However, at $|n-N| = 3$, the deviation becomes manifest when $\Delta\tau U > 0.5$, and even more terribly, the weight becomes negative.

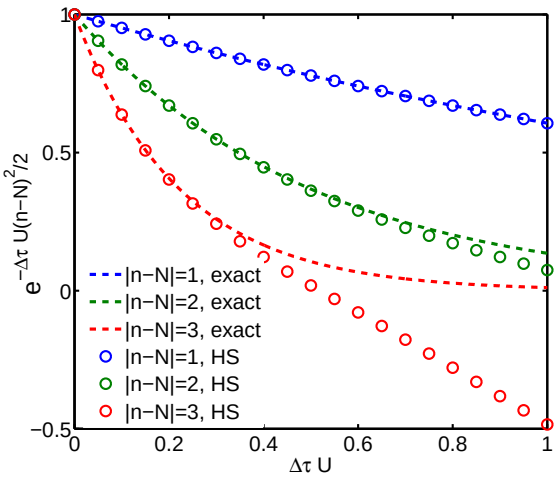

FIG. 1. Error due to the HS decomposition using parameters defined in Eq. 4. The dashed lines are exact results of $\mathrm{e}^{-\Delta\tau U(n_i-N)^2/2}$ with $|n-N| = 1, 2, 3$ respectively. The circles represent the results after the HS transformation.

Therefore, we design an exact HS decomposition for the cases from SU(2) to SU(6) in which the operator $n_i - N$ only takes eigenvalues among $0, \pm1, \pm2$, and ±3. The form of the new HS decomposition is the same as Eq. 4 but it is exact. The values of the discrete HS fields are defined as follows

$$\begin{aligned}
&\gamma(\pm1) = \frac{-a(3+a^2)+d}{d}, \qquad \gamma(\pm2) = \frac{a(3+a^2)+d}{d},\\
&\eta(\pm1) = \pm\cos^{-1}\left\{\frac{a+2a^3+a^5+(a^2-1)d}{4}\right\}\\
&\eta(\pm2) = \pm\cos^{-1}\left\{\frac{a+2a^3+a^5-(a^2-1)d}{4}\right\},
\end{aligned} \quad (5)$$

where $a = e^{-\frac{1}{2}\Delta\tau U}$, $d = \sqrt{8+a^2(3+a^2)^2}$. Eq. 5 is used for all of our simulations in 2D SU($2N$) Hubbard model in the main text.

After integrating out fermions, we arrive at the fermion determinant whose value depends on the discrete HS fields. The HS fields are sampled using the standard Monte Carlo technique.

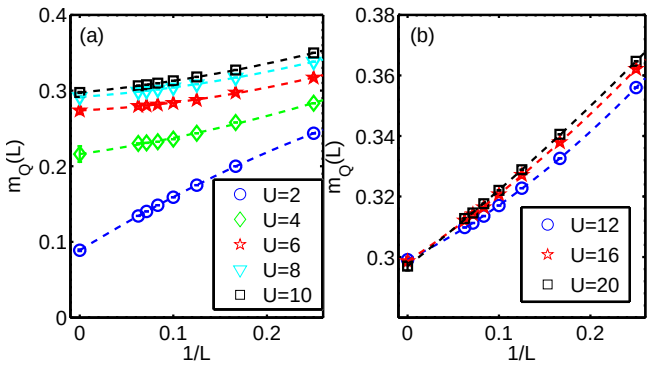

FIG. 2. Finite size scalings of $m_Q(L)$ v.s. $1/L$ for the half-filled SU(2) Hubbard model. The lines are fitted by the quadratic polynomial fitting of the QMC data. Error bars of QMC data are smaller than symbols.

II. TESTS OF THE PINNING FIELD METHOD

Below we present various tests of the pinning field method to confirm its validity and its sensitivity to weak orderings.

A. Test of the pinning field method in the half-filled SU(2) Hubbard model

We have performed the QMC simulations with the local pinning field method for the half-filled SU(2) Hubbard model in the square lattice. The finite-size scaling is presented in Fig. 2. The parameter values are the pinning field $h_{i_0 j_0} = 2$ and the projection time $\beta = 240$. The extrapolated values of the Neel moments m_Q defined in Eq. increase monotonically as U increases and become to saturate around $U = 10$. The Neel moment reaches 0.297 ± 0.002 at $U = 20$ in our simulation, which agrees well with previous QMC simulations. This test confirms the validity of the pinning field method.

B. Sensitivity of the pinning field method to weak ordering

We consider the cases of weak Neel ordering in the half-filled SU(6) Hubbard model in the square lattice with $U = 4$ and $U = 10$. The finite-size scalings based on structure factor are shown in Fig. 3. Quadratic polynomials are used to fit the structure factor $S(Q)/L^2$ as defined in Ref. 5. It is difficult to conclude whether long-range Neel ordering exists or not in both cases. In contrast, for the case of $U = 4$, the finite-size scaling based on the pinning field method in Fig. 1 in the main text yields the extrapolated Neel moment $m_Q = 0.026$. The corresponding value of $S(Q)/L^2$ is its square at the order of 10^{-3} and thus is too weak to identify in Fig. 3. Moreover, for the case of $U = 10$ in which the largest

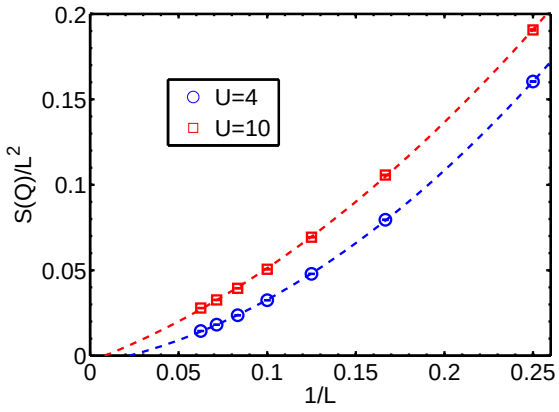

FIG. 3. Finite size scalings of the structure factor $S(Q)/L^2$ in the case of SU(6) with $U = 4$ and $U = 10$. Quadratic polynomials are used to fit the data. Error bars of QMC data are smaller than symbols. In these calculations, projection time $\beta = 80$ is used.

Neel moment appears (Fig. 4 in the main text), the corresponding structure factor remains too small to be extrapolated through the finite size scaling. The weak Neel orderings in the SU(6) Hubbard model were not found in a previous work based on the structure factor method by some of the authors either[5]. Due to the improved numeric resolution, they are identified through the pinning field method.

C. The pinning field method for the 1D SU(2) and SU(4) Hubbard models

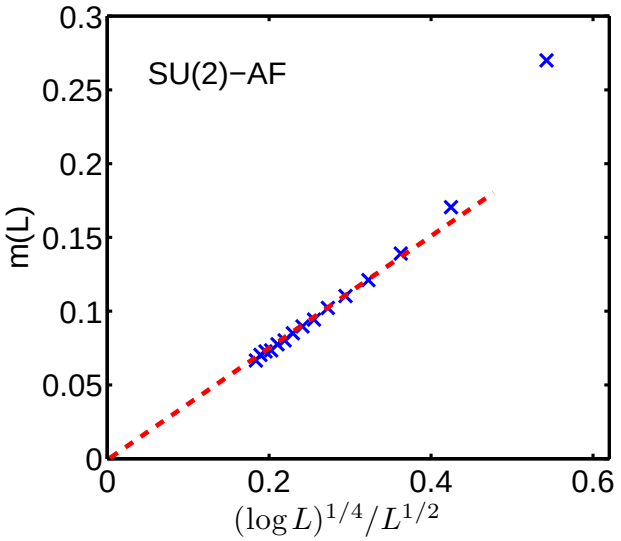

FIG. 4. Finite size scaling of $m(L)$ v.s. $(\log L)^{\frac{1}{4}}/L^{\frac{1}{2}}$ for the 1D half-filled SU(2) Hubbard model. Parameter values are $\beta = 80$, $U = 4$ and $h_{i_0 j_0} = 2$.

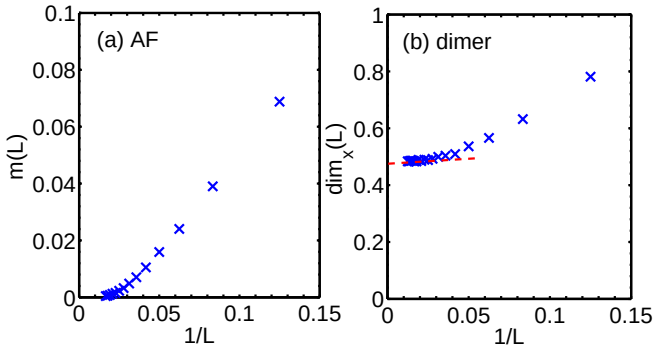

FIG. 5. (a) Finite size scaling of $m(L)$ v.s. $1/L$ for the 1D half-filled SU(4) Hubbard model. (b) Finite size scaling of $\dim_x(L)$ v.s. $1/L$ for the 1D half-filled SU(4) Hubbard model. Parameter values are $\beta = 80$, $U = 4$ and $\Delta t_{i_0 j_0} = 2$.

Since the pinning field method is sensitive to weak long-range orderings, a natural question is that whether it is oversensitive. To clarify this issue, we apply it to 1D half-filled SU(2) and SU(4) Hubbard models in which it is well-known that magnetic long-range orders do not exist. The QMC simulation results presented below are in an excellent agreement with previous analytic and numeric results. This confirms the validity of the pinning field method. We use the pinning fields described in the Eq. 3 and Eq. 5 in the main text to investigate Neel and dimer orderings, respectively.

For the 1D half-filled SU(2) Hubbard model, the pinned sites are set as $i_0 = 1$ and $j_0 = 2$, respectively, and values of the pinning fields are $h_{i_0,j_0} = 2$. We consider the induced magnetic moment on the furthest sites $\frac{L}{2}$ and $\frac{L}{2}+1$ defined as $\pm m(L)$. Strong quantum fluctuations suppress the long-range Neel ordering, and the asymptotic behavior of the two-point spin correlation functions at half-filling follows the pow-law decay as[6]

$$\langle S(i)S(j)\rangle \sim (-)^{i-j}\frac{\log^{\frac{1}{2}}|i-j|}{|i-j|}. \tag{6}$$

Since spin moments are pinned at i_0 and j_0, $m(L)$ should scales as

$$m(L) \sim \frac{(\log L)^{\frac{1}{4}}}{\sqrt{L}}. \tag{7}$$

Our QMC results with pinning fields are in an excellent agreement with Eq. 6 as shown in Fig. 4.

The magnetic properties of the 1D half-filled SU(4) Hubbard model are dramatically different from the SU(2) case. Bosonization analysis[7] shows that its ground states exhibit long-range-ordered dimerization with a finite spin gap, and the Neel correlation decays exponentially. We set the pinned sites at $i_0 = 1$ and $j_0 = 2$, respectively, and the pinning field for dimerization as $\Delta t_{i_0 j_0} = 2$. The induced dimer order is defined as the difference between two furthest bonds $(\frac{L}{2}, \frac{L}{2}+1)$ and $(\frac{L}{2}+1, \frac{L}{2}+2)$ as

$$\dim_i(L) = (-)^i\{d_{L/2,x} - d_{L/2+1,x}\}. \tag{8}$$

Our QMC simulation results are illustrated in Fig. 5 (b), which exhibit the long-range ordering in agreement with previous analytic results.

D. The issue of non-linear response to the pinning field

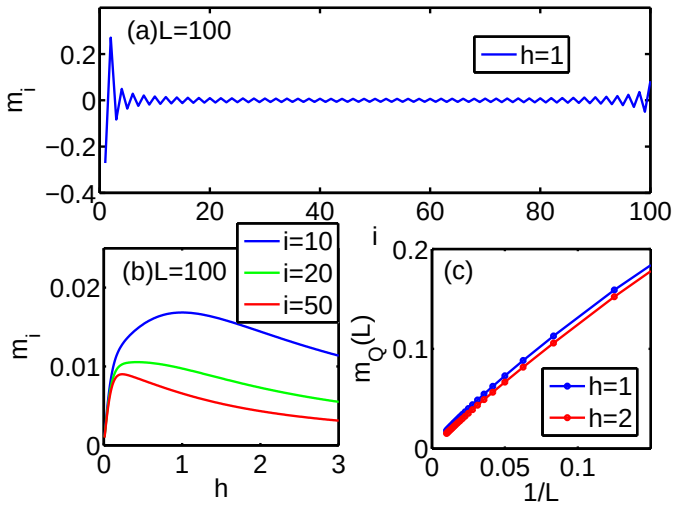

FIG. 6. The induced magnetic moments $m(i)$ by pinning fields in the non-interacting half-filled 1D SU(2) lattice model. (a) The spacial distribution of $m(i)$ with $h_{i_0 j_0} = 1$ and $L = 100$. (b) The induced moments $m(i)$ v.s h_{i_0,j_0} at different sites $i = 10, 20$ and 50 in the system with $L = 100$. (c) The scaling of $m_Q(L)$ with $Q = \pi$ at two different pinning fields.

In Fig. 1 of the main text, we present the scaling of the residual Neel moment $m_Q(L)$ *v.s.* $1/L$ with two different values of the pinning fields. A counter-intuitive observation is that $m(L)$ is weaker at $h_{i_0 j_0} = 2$ than that of $h_{i_0 j_0} = 1$. Below we present convincing evidence that actually this is not an artifact of the finite size. This is a typical behavior of responses on sites far away from the scattering center in the strong scattering limit.

To illustrate this point, we present the calculation for a toy model of a non-interacting half-filled SU(2) 1D lattice system, such that we can easily calculate systems with very large size up to $L = 100$. The pinning fields are located at sites $i_0 = 1$ and $j_0 = 2$, and the induced magnetic moments $m(i)$ are presented in Fig. 6. Although it is natural that the induced magnetic moments increase monotonically with h right on the impurity sites, there is no reason to expect the same behavior on sites away from the scattering center. On these sites, in fact, Fig. 6(b) shows that $m(i)$'s are non-monotonic with respect to h. All of them decays at large values of h after passing maxima at intermediate values of h. The finite size scalings of $m_Q(L)$ defined in the main text are presented in Fig. 6(c) at $h = 1$ and 2. Both curves converge

quantity	QMC	ED
$\langle m(1,1)\rangle_{U=4}$	0.4340±0.0001	0.4342
$\langle m(3,3)\rangle_{U=4}$	0.2344±0.0003	0.2351
$\langle m(1,1)\rangle_{U=12}$	0.4796±0.0001	0.4807
$\langle m(3,3)\rangle_{U=12}$	0.3207±0.0002	0.3218
$\langle m(1,1)\rangle_{U=20}$	0.4902±0.0001	0.4915
$\langle m(3,3)\rangle_{U=20}$	0.3248±0.0002	0.3261

TABLE I. The induced magnetic moments $m(1,1)$ and $m(3,3)$ by the pinning fields for the half-filled SU(2) Hubbard model. Both the QMC and exact diagonalization results are presented for comparison. The parameter values are $h_{i_0 j_0} = 2$, $\beta = 240$, $\Delta\tau = 0.05$. The lattice size is 4×4.

to 0 as they should be in non-interacting systems. Again, the curve with $h = 2$ is lower than that of $h = 1$.

III. ERROR ANALYSIS

In this section, we present the comparisons with exact diagonalization, the analyses on errors from the discrete Suzuki-Trotter decomposition and finite projection time β.

A. Comparison with the exact diagonalization

In order to check the numeric accuracy of our simulations, we first compare our QMC results with the pinning fields in the SU(2) case with those from the exact diagonalization in the 4×4 lattice.[8] The pinning fields are applied at sites $i_0 = (1,1)$ and $j_0 = (2,1)$ according to Eq. 3 in the main text. In table. I, we list the magnetic moments on sites $(1,1)$ and $(3,3)$ with different U's. As U goes up, the numeric errors of QMC increase, but are still less than 0.002 even at $U = 20$.

B. Scaling on the discrete $\Delta\tau$

For the Suzuki-Trotter decomposition defined in Eq. 2, its error is at the order of $tU^2(\Delta\tau)^3$. Such an error is most severe in the large U regime, and thus we only present the scaling with respect to $\Delta\tau$ at $U = 20$.

The pinning fields are chosen in the same configuration described in Eq. 3 in the main text. The distribution of m_i is staggered with decaying magnitudes as away from two pinned sites i_0 and j_0. The weakest moments are located at the central points $(\frac{L}{2}+1, \frac{L}{2}+1)$ and $(\frac{L}{2}+2, \frac{L}{2}+1)$. The residual values at these two points are denoted as $\pm m(L)$, respectively. The long-range order can also be reached as the limit of $m(L)$ in the thermodynamic limit $L \to \infty$.

In Fig. 7, curves of the Neel moment $m(L)$ v.s. $\Delta\tau$ are plotted for the three cases of SU(2), SU(4), and SU(6),

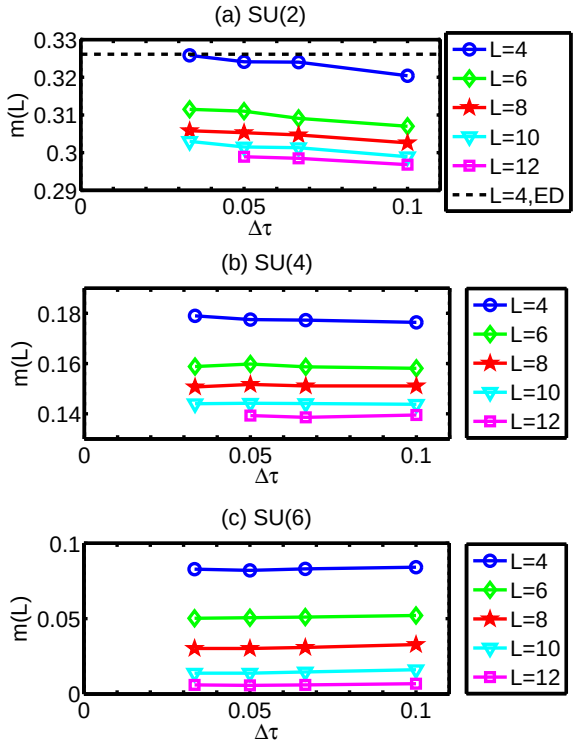

FIG. 7. Scaling of the Neel moments $m(L)$ v.s. $\Delta\tau$ for the cases of SU(2), SU(4) and SU(6) shown in (a)∼(c), respectively. In the case of SU(2), exact diagonalization results are also plotted as the dashed line for comparison. The parameters are $U = 20$, $\beta = 80$ and $h_{i_0 j_0} = 2$.

respectively. The slopes of these scaling lines are nearly independent on the lattice size L for all three cases. Due to convergence of the finite $\Delta\tau$ scaling, we use the value of $\Delta\tau = 0.05$ in all our simulations.

C. The finite β scaling

Next we check the effect of the finite projection time β. We use the residue Neel moment $m(L)$ at the furthest points for scaling as defined in Sect. III B. In Fig. 8, we present the scalings of the Neel moments $m(L)$ v.s. β for different sizes $L = 4, 6, 8$, and 10. For each curve, we define β_c as the convergence projection time after which $m(L)$ converges, and its approximate position is marked by an arrow. Here we only present the scalings at $U = 2$ in the weak coupling regime and at $U = 20$ in the strong coupling regime. The largest values of β_c are expected in either of these two limits, which can be understood as follows: β_c is determined by the finite gap of the many-body spectra. In the small U regime, the finite size gap increases as increasing U, while in the large U regime, it deceases as U increases because the energy scale is controlled by the magnetic exchange scale $J \sim 4t^2/U$.

In the case of SU(2), the relations of β_c's on L are

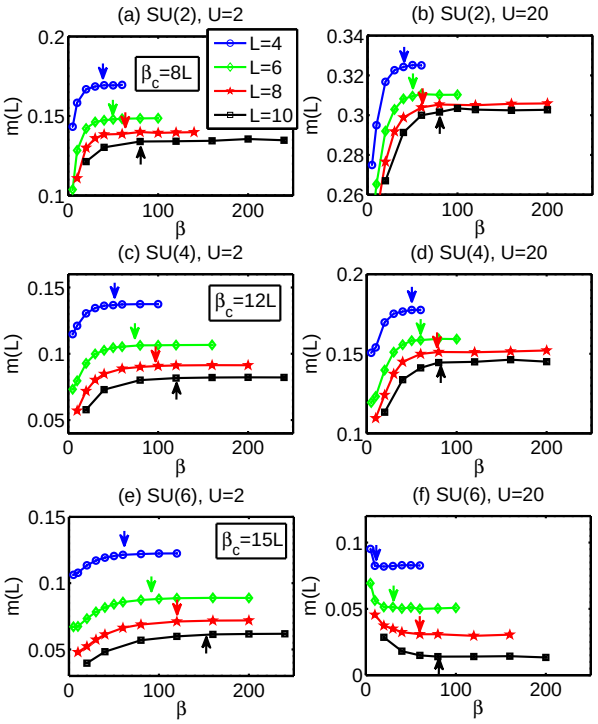

FIG. 8. The scalings of the Neel moments $m(L)$ v.s. β for the half-filled SU($2N$) Hubbard model. Lattice sizes are $L = 4, 6, 8, 10$. The interaction parameter for (a), (c), and (e) is $U = 2$, and that for (b), (d), and (f) is $U = 20$. Error bars of QMC data are smaller than symbols. The arrows mark the estimated convergence projection time β_c of these curves. The approximate relations of β_c v.s L are estimated as $\beta_c = 8L, 12L$ and $15L$ for the cases of SU(2), SU(4) and SU(6), respectively.

nearly the same for $U = 2$ and $U = 20$, which are estimated as $8L$. In the cases of SU(4) and SU(6), β_c's at $U = 2$ are larger than the corresponding ones at $U = 20$. At $U = 2$, their dependence on L is estimated as $\beta_c \approx 12L$ for the SU(4) case and $\beta_c \approx 15L$ for the SU(6) case, respectively. At $U = 20$, the system enters to the dimerization phase, and thus $m(L)$ is suppressed by longer projection time.

The largest size in our simulations is $L = 16$. Considering the above scalings, we choose $\beta = 15 \times 16 = 240$ for all the simulations presented in the main text, which should be sufficient to obtain accurate numeric results. In particular, the major result in the main text, i.e., the non-monotonic behavior of $m(L = \infty)$ with increasing U for both the SU(4) and SU(6) cases, is not an artifact from the finite projection time β.

[1] F. F. Assaad and H. G. Evertz, "Computational many-particle physics," (2008).
[2] J. E. Hirsch, Phys. Rev. B **28**, 4059 (1983).
[3] F. F. Assaad, arXiv:cond-mat/9806307.
[4] C. Wu and S.-C. Zhang, Phys. Rev. B **71**, 155115 (2005).
[5] Z. Cai, H.-H. Hung, L. Wang, and C. Wu, Phys. Rev. B **88**, 125108 (2013).
[6] H. J. Schulz, Phys. Rev. Lett. **64**, 2831 (1990).
[7] C. Wu, Phys. Rev. Lett. **95**, 266404 (2005).
[8] We thank H. H. Hung for providing the results of exact diagonalization.